Advances in Geo-Energy Research

Vol. 5, No. 2, p. 127-138, 2021

Original article

Impact of permeability heterogeneity on geothermal battery energy storage

Palash Panja[1,2]*, John McLennan[1,2], Sidney Green[3,4]

[1]*Department of Chemical Engineering, University of Utah, Salt Lake City, Utah, United States*

[2]*Energy & Geoscience Institute, University of Utah, Salt Lake City, Utah, United States*

[3]*Enhanced Production Inc., Salt Lake City, Utah, United States*

[4]*Depeartment of Mechanical Engineering, University of Utah, Salt Lake City, Utah, United States*

Keywords:
Spatial heterogeneity
geothermal battery
heat recovery
bottom hole pressure
temperature distributions

Cited as:
Panja, P., McLennan, J., Green, S. Impact of permeability heterogeneity on geothermal battery energy storage. Advances in Geo-Energy Research, 2021, 5(2): 127-138, doi: 10.46690/ager.2021.02.03

Abstract:
In the emergence of new technologies to harness renewable energy, industrial-scale storage of heated water in a geothermal system is a promising technique. A porous, permeable medium, bounded by a poorly thermally conductive/convective overburden and underburden, can be used for transient subsurface thermal storage. The reservoir in this concept forms a geothermal battery. As a very simplified scenario, consider a single well injecting and producing hot water diurnally or seasonally. The source of the hot water could be solar-heated water, for example, or possibly even water heated from the excess regional electricity supply. For that situation, this study investigates the influence of spatial permeability heterogeneity on heat recovery, and the distributions of temperature and pressure inside the reservoir. Four heterogeneous models are created from lognormal distributions of permeability by varying the standard deviations while keeping the mean absolute permeability at 100 mD. The injection pressure experienced while pumping into a candidate formation is affected by heterogeneity; higher bottom hole pressure is required to inject water into a more heterogeneous reservoir. The spatial distribution of temperature is less affected by permeability heterogeneity. In the simulations carried out, 91% of the heat is recovered after the 30th cycle of injection/production operation in all cases proving less impact of heterogeneity on heat recovery for fixed injection and production rates.

1. Introduction

Geothermal subsurface settings are used directly for recreation, for indirect uses such as heating and certainly for generating electricity. It is proposed that surrogate geothermal reservoirs can also be engineering and used as a medium for storing hot water that is heated at a surface facility using excess electricity or direct solar heat (Wendt et al., 2019a, 2019b). This stored water can be produced back and converted to electricity on demand. This conceptual geothermal system is known as geothermal battery energy storage. In previous studies (Green et al., 2020; Panja et al., 2020), it has been demonstrated that geothermal battery is a potential technology for storing hot water in high permeability and porosity formations during periods of adequate solar radiance. The water can be produced for power generation when necessary (diurnally or seasonally) and subsequently the same water can be reinjected after a subsequent heating cycle at the surface. This operation of injection and production in the same well is often known colloquially as "huff and puff".

Many factors that control the functionality of such a system in a homogeneous reservoir have been addressed elsewhere (Wendt et al., 2019a, 2019b; Green et al., 2020; Panja et al., 2020, 2021). However, heterogeneity or geostatistical distribution of geologic parameters such as permeability has been shown to have a major impact on the fluid flow in porous media. Heterogeneity in any property is a natural characteristic of a porous medium that occurs due to slow deposition and mixing of various materials over a long period. The heterogeneity is prominent on a microscopic scale rather than a field scale. Therefore, the heterogeneity in a nano-porous medium such as shales or tight formation often has

*Corresponding author.
E-mail address: ppanja@egi.utah.edu (P. Panja); jmclennan@egi.utah.edu (J. McLennan); sgreen@xmission.com (S. Green).

Yandy Scientific Press

2207-9963
Received February 20, 2021; revised March 1, 2021; accepted March 1, 2021; available online March 3, 2021.

Table 1. List of base parameters for the formation, overburden, and underburden (Panja et al., 2020).

Parameters	Formation	Overburden/Underburdon
Specific heat of rock (J/(Kg-K)	930	770
Thermal conductivity (W/(m-K)	2.5	1.05
Density (kg/m^3)	2,000	2,500
Mean horizontal permeability, k_x and k_y (mD)	100	0.0001
Vertical permeability, k_z (mD)	0.1 k_x	0.0001
Porosity (%)	15	2.5
Initial temperature (°C)	120	120
Initial pressure (MPa)	12	12
Formation thickness (m)	110	70

a major impact on production. A fine grid reservoir model is required to capture heterogeneity at this microscopic level. This requires huge computational power and time. Practically, the numerical model is developed by upscaling these properties like permeability and porosity for better performance. The heterogeneity on the microscopic or nanoscopic scale is often lost in this numerical operation. Several studies consider the consequences of permeability heterogeneity on the production of hydrocarbons (Hopkinson et al., 1960; Gupta et al., 1988; Assadoor et al., 1989; Newley and Begg, 1992; Yang and Butler, 1992; Ehlig-Economides et al., 2004; Li and Xie, 2011; Naderi et al., 2015; Aragón-Aguilar et al., 2017; Ashley et al., 2017). However, only a few studies are available for heterogeneity in a geothermal reservoir.

Researchers from the National Renewable Energy Laboratory showed that, depending on the specifics, the total flow rate of methane and brine in a geo-pressured geothermal reservoir can be higher in a layered situation compared to a homogeneous reservoir with the same mean permeability (Esposito and Augustine, 2012). Crooijmans et al. (2016) considered the impact of heterogeneity on energy extraction for a low-temperature geothermal doublet system. Permeability and porosity heterogeneity greatly affected CO_2 migration (Xu et al., 2017; Wang et al., 2019) and the produced water temperature and heat recovery (Li et al., 2019). Pandey et al. (2015) showed the influence of reservoir permeability heterogeneity during geothermal heat extraction. Another study showed the effect of permeability on heat transfer and permeability evolution in an enhanced geothermal system using a fully implicit thermal simulator (Ijeje et al., 2019). However, none of these publications considered a single well injection/production scheme in porous formation for a geothermal energy storage system. In our previous study (Panja et al., 2021), it is shown that the heat recovery for a given cycle is not affected significantly by permeability anisotropy and layering of the storage medium. In this study, we investigate the effects of permeability heterogeneity on geothermal battery functionality.

2. Reservoir model and heterogeneity

Simultaneous flows of heat and fluid in porous media are numerically calculated using a commercial thermal simulator; STARS from the Computer Modeling Group, Calgary, Canada (CMGL, 2021). The heat and fluid flow equations used in STARS are summarized in Appendix A. A surrogate porous medium for potential hot water storage (formation) is created with insulating overburden and underburden zones. 25 layers (10 meters of true vertical thickness each) constitute the model; 7 layers for the overburden, 11 layers for the target formation and, 7 layers for the underburden. The overburden and underburden have low porosity (2.5%) and low permeability (100 nD) compared to the target formation (15% porosity and 100 mD permeability). The geologic and thermophysical parameters are consistent with a previous study (Panja et al., 2020) and are shown in Table 1.

The dimensions and the three segments (underburden, overburden, and formation) of the numerical reservoir model are shown in Fig. 1. The numerical model is 200 meters in $x-$ and 200 meters in $y-$directions. The formation thickness is 110 meters and the overburden and the underburden have

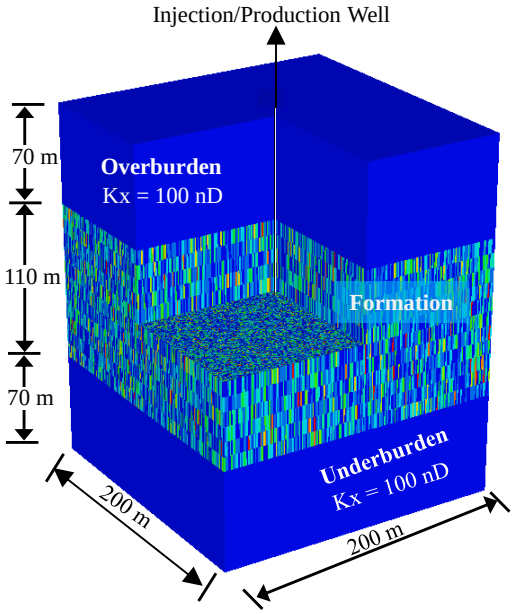

Fig. 1. The reservoir model showing the three segments namely overburden, formation and underburden with the dimensions and heterogeneity in permeability.

Table 2. The data and lognormal distribution parameters used for assessing the role of spatial permeability heterogeneity.

Distribution No.	Data distribution parameters			Lognormal distribution parameters	
	μ_N (mD)	σ_N (mD)	CV= σ_N/μ_N	μ	σ
1	100	25.38	0.2538	4.574	0.25
2	100	53.29	0.5329	4.480	0.50
3	100	86.90	0.8690	4.324	0.75
4	100	131.07	1.3107	4.105	1.00

70 meters thickness each. The well is drilled in the middle of the formation with the perforations in the formation layers only.

There are several methods such as Kriging, gaussian geostatistics to create a heterogeneous distribution of a property over a space. We have adopted the gaussian unconditional geostatistical method in this study to create permeability heterogeneity in the formation layer. The primary information for this method is to obtain a probability distribution of permeability. Several studies proved that absolute permeability in porous media is commonly characterized by a lognormal distribution(Vargas-Guzmán, 2009; Kusanagi et al., 2015).

Four different lognormal distributions of permeability are chosen, each with a mean of 100 mD. The lognormal distribution parameters, μ and σ, are computed from the mean, μ_N, and standard deviation, σ_N, of a lognormal random variable, as shown in Eqs. (1) and (2).

$$\mu = \ln \frac{\mu_N^2}{\sqrt{\sigma_N^2 + \mu_N^2}} \tag{1}$$

$$\sigma = \sqrt{\ln\left(\frac{\sigma_N^2}{\mu_N^2} + 1\right)} \tag{2}$$

The probability density function of the lognormal distribution is given by Eq. (3).

$$y = f(x|\mu,\sigma) = \frac{1}{x\sigma\sqrt{2\pi}} \exp\left[-\frac{(\ln x - \mu)^2}{2\sigma^2}\right], \quad \text{for } x > 0 \tag{3}$$

The mean (μ_N) of all distributed data is kept fixed at 100 mD and the standard deviation (σ_N) is varied as shown in Table 2. The coefficient of variation (CV), defined by the ratio of standard deviation and mean of the distribution, is also shown in Table 2.

The four lognormal distributions of permeability are compared in Fig. 2. The permeability for a scenario with completely homogeneous and isotropic permeability is shown as a vertical line.

As seen in Fig. 2, the distributions of absolute permeability are skewed towards progressively lower values with increasing standard deviation. Therefore, the mean of the lognormal distribution also decreases with increasing standard deviation.

In the gaussian unconditional geostatistical method, the values of permeability are randomly drawn from a predefined lognormal distribution which is a possible representation of

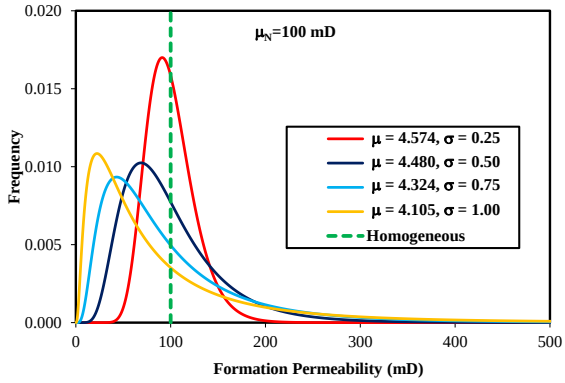

Fig. 2. Lognormal distribution of permeability.

the field. These values are then assigned to each grid of the numerical reservoir model as shown in Fig. 1. While varying spatially (from element to element), at any point, the permeability is the same in all horizontal directions. At each element, there is a fixed anisotropic absolute permeability ratio ($k_x/k_z = 10$) in the vertical direction. The overburden and underburden segments are specified with spatially independent and completely isotropic absolute permeability. Geostatistical distributions (realization 1) from the four lognormal distributions on an $x-y$ plane at mid-height of the target storage formation are shown in Fig. 3.

Mathematically, very low to very high values of permeability can be obtained from the four distributions. However, in a field, it is not very common to observe permeability beyond some limiting values. Therefore, the permeability values from the lognormal distribution are chosen in the range of 10-400 mD to encompass feasible field scenarios. Values outside of this range are not assigned to any grids of the reservoir model.

In the unconditional gaussian geostatistical method, several sets of permeabilities can be mathematically created from a single distribution for all grids of the storage layer. These sets are statistically identical. However, each set of permeability can be arranged geostatistically (spatially) in several ways that are denoted as realizations. Consequently, each creates a unique spatial distribution of permeability that leads to a different reservoir model. Ideally, averaging of numerical results from hundreds of such models would be able to represent the effects of heterogeneity. In this study, five realizations are created for each distribution for practical purposes to reduce the total simulation run time. Temperature, pressure profiles,

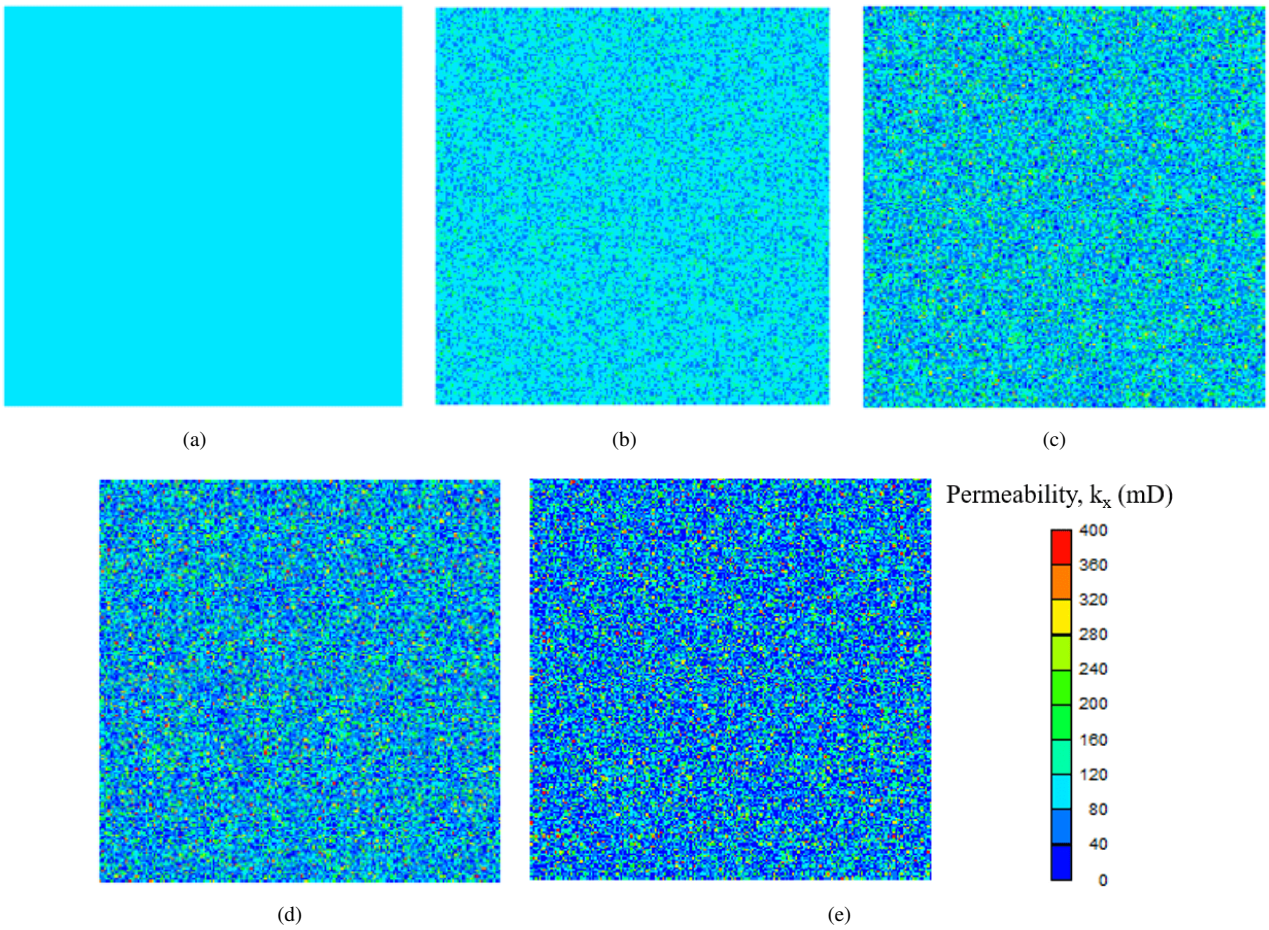

Fig. 3. Spatial distribution of permeability of realization 1 (out of 5 realizations) from (a) homogeneous, k_x = 100 mD; (b) distribution 1; (c) distribution 2; (d) distribution 3; (e) distribution 4.

and heat recovery from all five of the realizations for each distribution are averaged. Because, the layers in the numerical reservoir model are refined in the $x-$ and $y-$ directions near the wellbore for better numerical stability and accuracy, the average permeability is determined based on the volumetric average for each grid, as shown in Table 3.

Once the models are built, a vertical well is placed in the middle of the reservoir with perforations covering the entire target formation only (middle segment in Fig. 1). A constant pressure boundary condition is used in these calculations. Other boundary conditions could have been selected to represent different field scenarios (for example, multiple wells with five-spot injection patterns). The analogy is to view the reservoir as being surrounded by an aquifer with pressure support. The reservoir is initially filled with connate water at 120 °C. The same well is mathematically envisioned as an injection well and a production well at different times in an injection/production/shut-in cycle. Water at 250 °C is injected for 8 hours at a rate of 40 kg/s. The same mass of water is produced for a longer time (10 hrs) at a slower rate of 32 kg/s. The well is then shut-in for 6 hours to complete a daily cycle. This schedule is numerically repeated for 30 days (or 30 cycles).

3. Results and discussion

The results of this suite of simulations are discussed with an emphasis on the temperature and pressure distributions inside the formation after the end of injection and, production of the 30th cycle. The amount of heat recovered after each cycle is also calculated. Additionally, the evolution of the bottom hole temperature and pressure with the number of cycles is assessed.

3.1 Pressure

Pressure distributions at the mid-height of the injection formation in the $x-y$ plane (horizontal plane and a vertical wellbore) are shown in Fig. 4 after the end of injection in the 30th cycle. The figure synthesizes four different permeability distributions and a homogeneous case.

As would be intuitively anticipated, the pressure at the wellbore is higher for a distribution with a higher standard deviation. As seen in Table 3, the volumetrically averaged permeabilities decrease with an increasing standard deviation of the lognormal distribution; i.e., 100, 99.5, 94.5, and 86.7 mD for distribution 1, distribution 2, distribution 3 and distribution 4, respectively. Therefore, higher pressure is required to inject the same amount of water in the lower permeability

Table 3. Mean and average permeability of each realization from four distributions.

Distribution	Realization	Distribution mean, μ_N (mD)	Volume average permeability (mD)
1	1	100	99.98
	2	100	99.96
	3	100	100.02
	4	100	100.03
	5	100	99.95
2	1	100	99.50
	2	100	99.53
	3	100	99.64
	4	100	99.51
	5	100	99.45
3	1	100	94.39
	2	100	94.49
	3	100	94.52
	4	100	94.37
	5	100	94.49
4	1	100	86.74
	2	100	86.70
	3	100	86.68
	4	100	86.67
	5	100	86.46

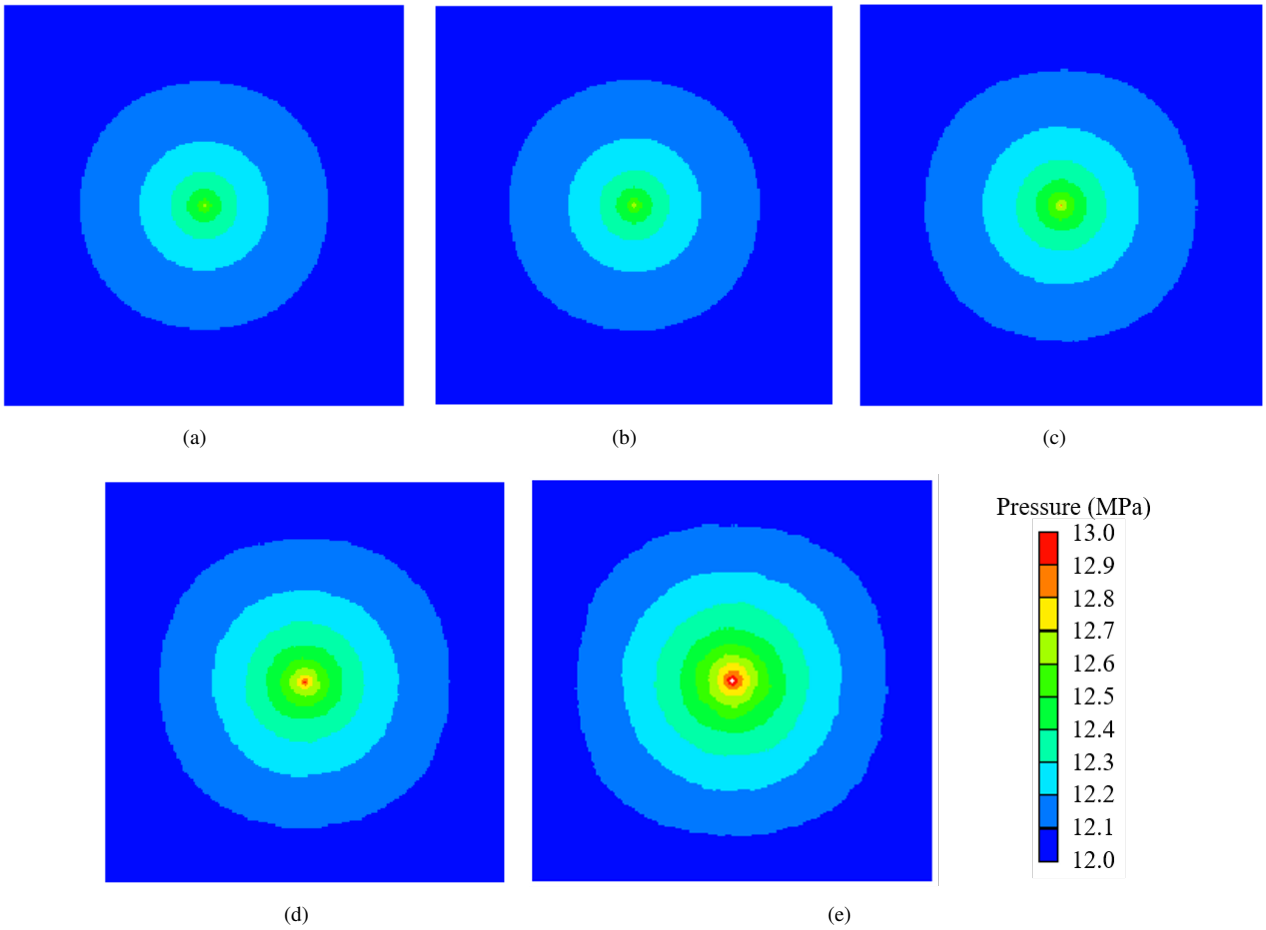

Fig. 4. Spatial distribution of pressure (MPa) at the end of injection in the 30th cycle of operation on the $x-y$ plane (200 meters×200 meters) at the mid-height of the formation for heterogeneity from (a) homogeneous; (b) distribution 1; (c) distribution 2; (d) distribution 3; (e) distribution 4.

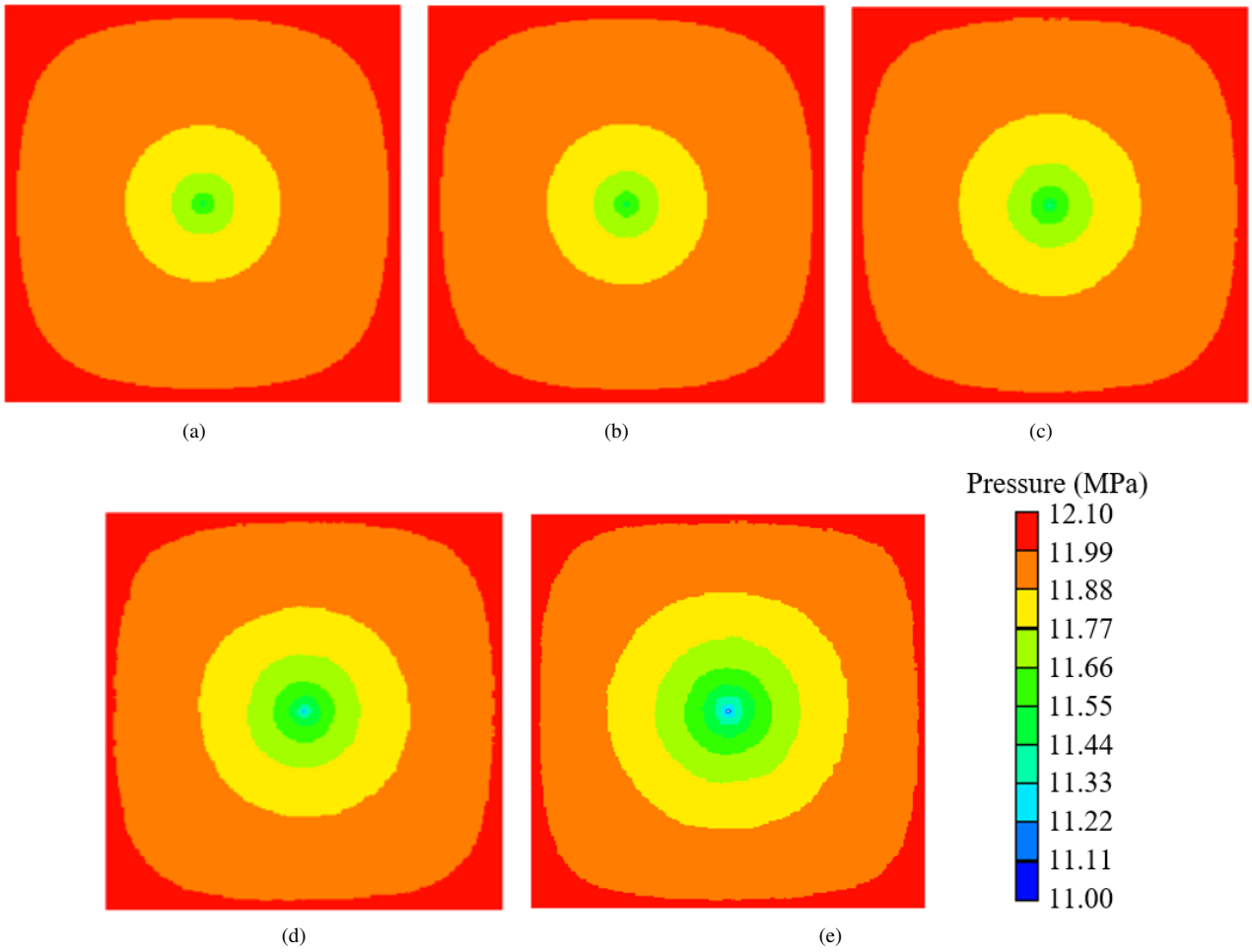

Fig. 5. Spatial distribution of pressure (MPa) at the end of production of the 30th cycle of operation on the $x-y$ plane (200 meters×200 meters) at the mid-height of the formation for heterogeneity from (a) homogeneous; (b) distribution 1; (c) distribution 2; (d) distribution 3; (e) distribution 4.

reservoir. As a result, elevated pressure fronts propagate farther towards the boundary with the increasing standard deviation of the lognormal distribution (i.e., from distribution 1 to distribution 4) at the end of the injection operation. The spatial distributions of pressure on the $x-y$ plane at the mid-height of the formation after the end of production in the 30th cycle are shown in Fig. 5.

The lowest pressure is required at the wellbore for the lowest average permeability in distribution 4 due to the requirement of the higher drawdown to produce the same amount of water. The pressure along a linear path in the $x-$direction at the mid-height of the formation is shown in Fig. 6.

The pressure front moves farther for distribution 4 having a higher standard deviation and lower mean permeability. The homogeneous case and distribution 1 have similar pressure profiles since the average permeabilities are almost the same. In Fig. 6(a), for example, the 12.3 MPa pressure front moves 17.0, 17.8, 22.8, 29.9, and 38.5 meters for homogeneous, distribution 1, distribution 2, distribution 3, and distribution 4, respectively.

At the end of production in the 30th cycle, the pressure at the wellbore is the lowest and increases towards the boundary-this is expected. Permeability distribution 4 demonstrates the lowest pressure, consistent with the lowest average permeability. Tracking the 11.7 MPa pressure front, it moves 8.8, 9.5, 13.2, 19.2, and 27.2 meters for homogeneous, distribution 1, distribution 2, distribution 3, and distribution 4, respectively.

The variations of the bottom hole pressure during injection and production during 30 days (i.e., 30 cycles) of operations are shown in Fig. 7.

The range of bottom hole pressure (injection to production) increases with the increasing standard deviation in lognormal distribution due to the lower average permeability. Therefore, the lowest bottom hole pressures during production and the highest bottom hole pressures during injection are required for distribution 4 having the lowest average permeability. In a single case, the injection pressure decreases and the production pressure increases slowly in the first few cycles. The pore volume near the wellbore expands under high pressure to accommodate the injected water. The rock also expands due to heating by the injected hot water, compensating, presumably at least partially, for the competing pore volume expansion. After the initial injection of hot water in the first few cycles, the temperature of the grains (a solid component of the reservoir) reaches a steady value as discussed in the next section. Therefore, the rock doesn't locally expand further due

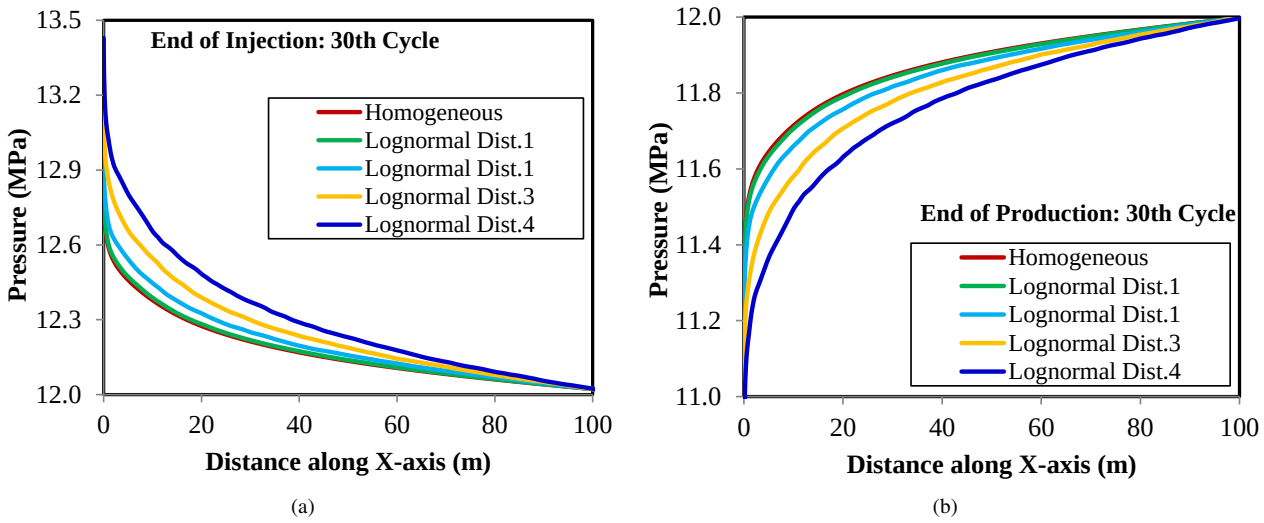

Fig. 6. Pressure profiles along $x-$direction from the middle of the formation for different heterogeneity after the 30th cycle of operation at the end of (a) injection; (b) production.

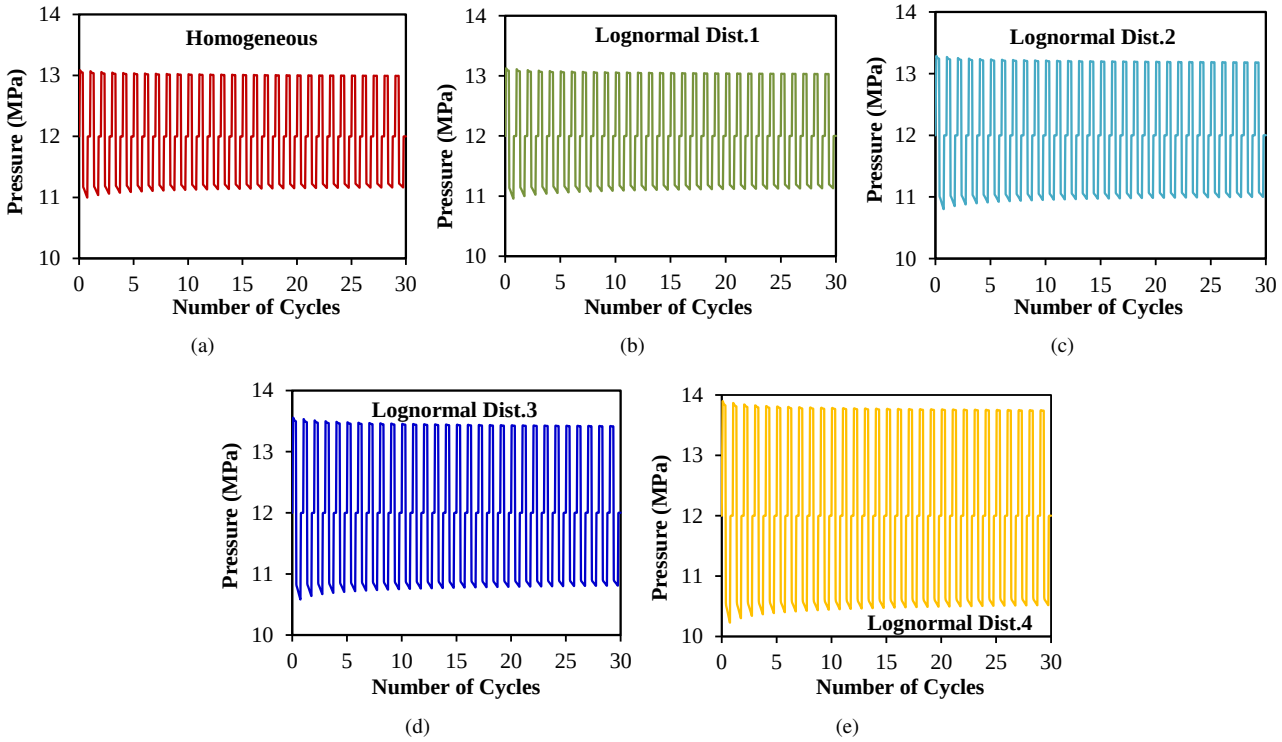

Fig. 7. Bottomhole pressure at the mid-height of the formation versus cycles of operation for heterogeneity from (a) homogeneous; (b) distribution 1; (c) distribution 2; (d) distribution 3; (e) distribution 4.

to heating with additional cycles. Consequently, the injection and production pressures are almost stabilized (i.e., reach a constant value) after 10 cycles of operation. Due to the relatively higher permeability of the formation (around 100 mD) and the constant boundary pressure condition, the pressure disturbance in the formation during injection and production doesn't last long after shutting-in. Hence, the pressure rapidly goes back to the initial reservoir pressure (12 MPa) during the shut-in.

3.2 Temperature

The temperature distributions at the mid-height of the target formation in the horizontal $x-y$ plane are shown in Fig. 8 after the end of injection in the 30th cycle. Temperature distributions are shown for four different permeability distributions.

On a smaller scale (grid-scale), the temperature variations are observed in all directions. However, overall it is not dominant in any direction. The spatial distributions are almost identical. This is due to the random distribution of permeability

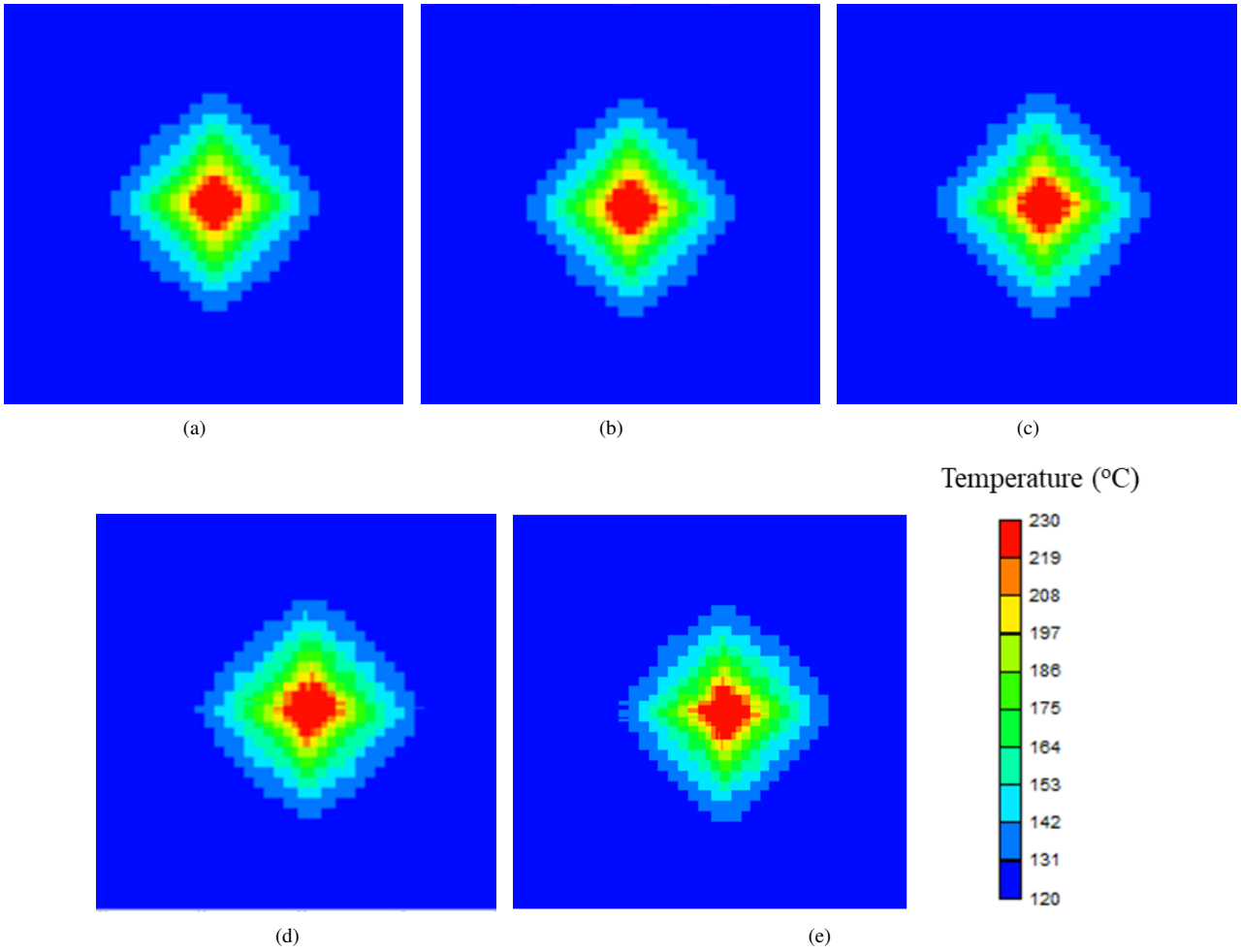

Fig. 8. Spatial distribution of temperature at the end of injection for the 30th cycle of operation on the $x-y$ plane (80 meters×80 meters) at the mid-height of the formation for heterogeneity from (a) homogeneous; (b) distribution 1; (c) distribution 2; (d) distribution 3; (e) distribution 4.

without any localized higher or lower permeability regions. Absolute permeability in a high permeability reservoir is intrinsic to that reservoir and independent of the type of fluid flowing through the porous rock. Although permeability is a characteristic flow property of porous rock, it doesn't affect the conductive heat transfer. Permeability does affect the convective heat transfer. Therefore, the temperature profile is primarily affected by heat carried with the hot water in the direction of the locally higher permeability. As a consequence, the temperature profiles shown in Fig. 8 are dominated by the local distribution of the permeability. The temperature distributions at the mid-height of the formation in the $x-y$ plane are shown in Fig. 9 after the end of production in the 30th cycle for four different permeability distributions.

The spatial temperature distributions after production are similar to those shown in Fig. 8 except that the temperatures are lower as hot water near the wellbore is produced and relatively colder in-situ water (120 °C) flows towards the wellbore. The variations of the bottom hole temperature during injection and production operations with the number of cycles are shown in Fig. 10.

As discussed earlier, permeability heterogeneity has a limited effect on the temperature profile. No significant differences are noticed in the bottom hole temperature for the different heterogeneities. The bottom hole temperature at the end of the injection reaches the injection water temperature (250 °C) after each cycle. During injection, the connate water (120 °C) displaced radially and the injected water (250 °C) moves in with an assumption of no significant mixing or fingering. Similarly, during production, hot water in the near-wellbore region is produced first, compelling the relatively cold water from a distance to move towards the wellbore. As a consequence, the wellbore reaches a lower temperature after the end of production. However, as the reservoir is being heated in every cycle due to less recovery of heat, the temperature of the surrounding water near the wellbore also increases. Therefore, the bottom hole temperature after the end of a production event increases with the number of cycles. The increment is slowly diminished as the heat transfer reaches a steady value after a few cycles (around 25 cycles).

3.3 Heat recovery

The cumulative heat recoveries from the heterogeneous reservoir created from 4 different distributions and a homoge-

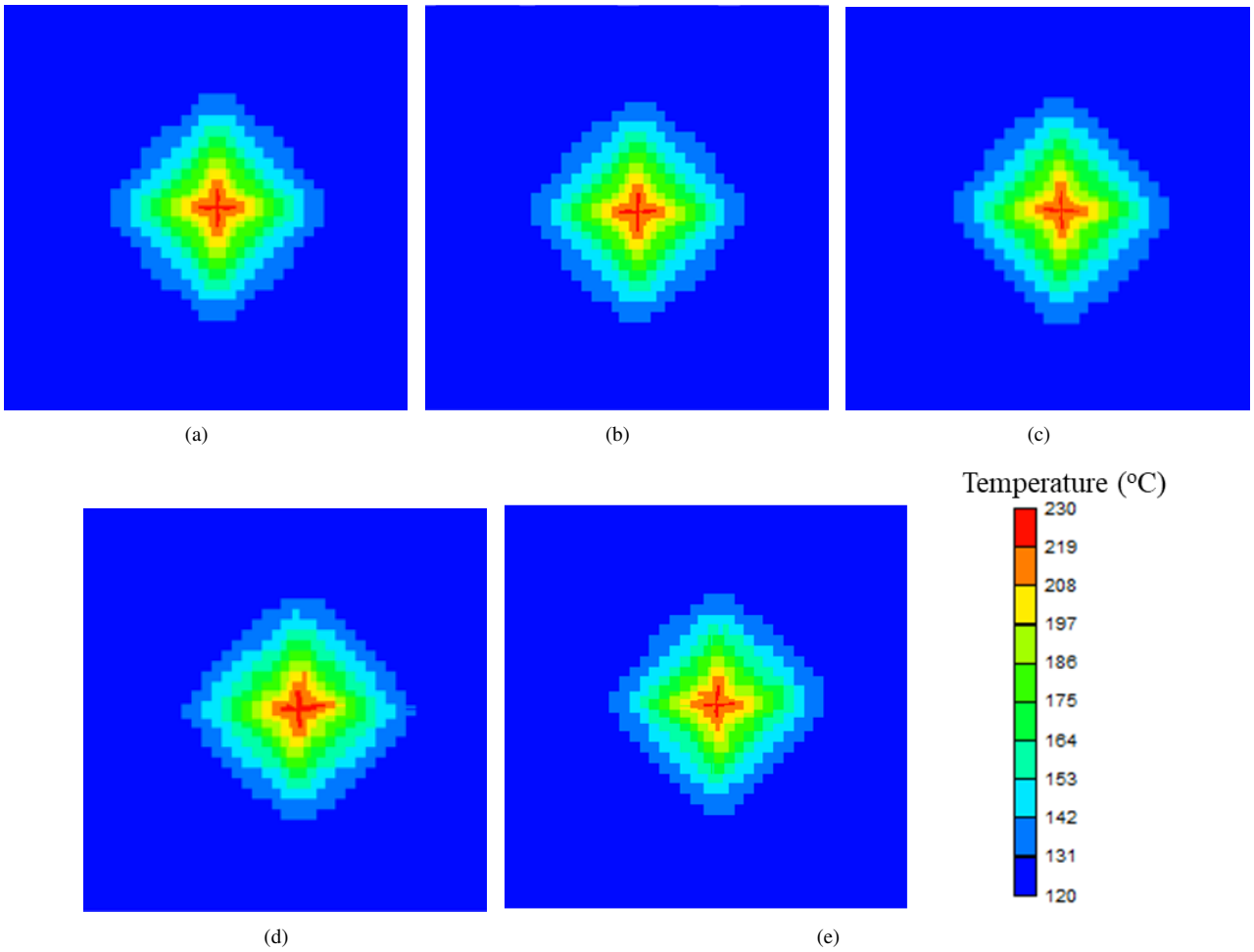

Fig. 9. Spatial distribution of temperature at the end of production of the 30th cycle of operation on the $x-y$ plane (80 meters×80 meters) at the mid-height of the formation for heterogeneity from (a) homogeneous; (b) distribution 1; (c) distribution 2; (d) distribution 3; (e) distribution 4.

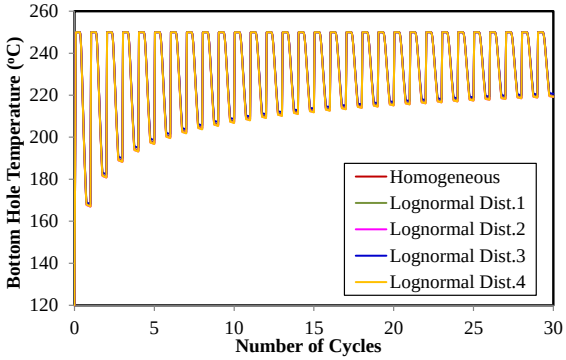

Fig. 10. Bottom hole temperature at the mid-height of the formation versus cycles of operation for different heterogeneities and a homogeneous case.

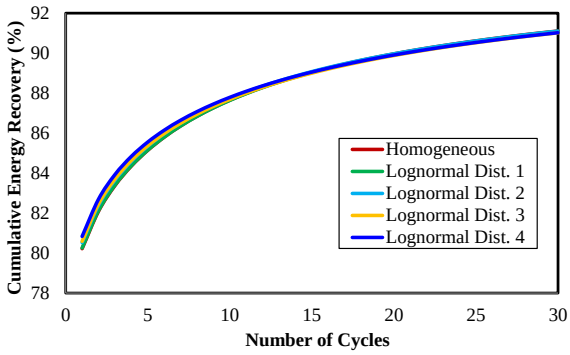

Fig. 11. The cumulative energy recoveries from heterogeneous reservoirs from four geostatistical distributions of permeability and a homogeneous reservoir.

neous reservoir are shown in Fig. 11.

No significant differences in cumulative heat recoveries are observed among four heterogeneous and an equivalent homogeneous reservoir. As described in the previous section, the spatial variation in permeability has less effect on temperature distributions. Not surprisingly, the mean permeabilities for the different heterogeneous situations near the wellbore (about 30 meters) where the temperature change is observed during the injection and the production cycle are almost the same.

4. Conclusions

Four lognormal distributions with the average permeabilities of 100, 99.5, 94.5, and 86.7 mD and progressively increasing standard deviations are studied. The results from

five realizations of each distribution are averaged to obtain a better quality of representation of heterogeneity. In the "huff and puff" operation, hot water at 250 °C is injected for 8 hours at a rate of 40 kg/s using an injection well and then the same well is used to produce water at a rate of 32 kg/s for 10 hrs. The well is then shut-in for the rest of the day. The effects of heterogeneity on the geothermal battery energy storage using this huff-puff method are not significant.

Higher injection pressures are required for a heterogeneous reservoir with higher variability in permeability. The higher pressure fronts also move farther from the wellbore in this case. The temperature profile is less affected by permeability heterogeneity. Higher variability in lognormal distribution results in reduced average permeability. Therefore, higher pressure is required to pump at a fixed rate. Consequently, the initial pressure front travels more distances for higher bottom hole pressure leads to a longer initial pressure front. The spatial distributions of temperature for the different heterogeneities in permeability are almost identical because the same amount of water is injected and the permeability is a flow property and doesn't affect the heat transfer. The shut-in pressure after each cycle re-equilibrates at the constant boundary pressure (12 MPa) over the 6-hour timeframe due to the relatively high permeability. Heat recovery is not affected by the different heterogeneities in permeability and approximately 91% of the heat is recovered after the 30^{th} cycle in all cases.

The effects of heterogeneity may be different for different ranges of permeability and its distribution. The trends in bottom hole pressure, bottom hole temperature, and heat recovery are also affected by the well's operating conditions.

Acknowledgement

The U.S. National Science Foundation provided funding for this project under grant NSF-EAGER-1912670.

Conflict of interest

The authors declare no competing interest.

References

Ahmed, T. Reservoir Engineering Handbook. Amsterdam, Netherlands, Gulf Professional Publishing, 2010.

Aragón-Aguilar, A., Izquierdo-Montalvo, G., López-Blanco, S., et al. Analysis of heterogeneous characteristics in a geothermal area with low permeability and high temperature. Geoscience Frontiers, 2017, 8(5): 1039-1050.

Ashley, W. J., Panja, P., Deo, M. Surrogate models for production performance from heterogeneous shales. Journal of Petroleum Science and Engineering, 2017, 159: 244-256.

Assadoor, A. Y., Fawakhiri, A. Y., Taresh, S. H., et al. Problems encountered in simulating large heterogeneous reservoirs. Paper SPE 17940 Presented at the Middle East Oil Show, Bahrain, 11-14 March, 1989.

CMGL. Computer Modeling Group Ltd.

Crooijmans, R. A., Willems, C. J. L., Nick, H. M., et al. The influence of facies heterogeneity on the doublet performance in low-enthalpy geothermal sedimentary reservoirs. Geothermics, 2016, 64: 209-219.

Dake, L. P. Fundamentals of Reservoir Engineering. Amsterdam, Netherlands, Elsevier, 1983.

Ehlig-Economides, C. A., Laine, R. E., Oguntaee, B. Effect of areal heterogeneity on waterflood performance between parallel horizontal wells. Paper SPE 90346 Presented at the SPE Annual Technical Conference and Exhibition, Houston, Texas, 26-29 September, 2004.

Esposito, A., Augustine, C. The influence of reservoir heterogeneity on geothermal fluid and methane recovery from a geopressured geothermal reservoir. Paper SPE 53921 Presented at Thirty-Seventh Workshop on Geothermal Reservoir Engineering, Stanford, California, 30 January-1 February, 2012.

Green, S., McLennan, J., Panja, P., et al. Geothermal battery energy storage. Renewable Energy, 2021, 164: 777-790.

Gupta, A. D., Pope, G. A., Sepehrnoori, K., et al. Effects of reservoir heterogeneity on chemically enhanced oil recovery. SPE Reservoir Engineering, 1988, 3(2): 479-488.

Hopkinson, J. L., Natanson, S. G., Temple, A. P. Effects of reservoir heterogeneity on performance. Paper SPE 1581 Presented at the Fall Meeting of the Society of Petroleum Engineers of AIME, Denver, Colorado, 2-5 October, 1960.

Ijeje, J. J., Gan, Q., Cai, J. Influence of permeability anisotropy on heat transfer and permeability evolution in geothermal reservoir. Advances in Geo-Energy Research, 2019, 3(1): 43-51.

Kusanagi, H., Watanabe, N., Shimazu, T., et al. Permeability-porosity relation and preferential flow in heterogeneous vuggy carbonates. Paper SPWLA JFES 2015E Presented at the SPWLA 21st Formation Evaluation Symposium of Japan, Chiba, Japan, 13-14 October, 2015.

Li, F., Xu, T., Li, S., et al. Assessment of energy production in the deep carbonate geothermal reservoir by wellbore-reservoir integrated fluid and heat transport modeling. Geofluids, 2019, 2019: 8573182.

Li, K., Xie, R. Effect of heterogeneity on production performance in low permeability reservoirs. Paper SPE 143482 Presented at the SPE EUROPEC/EAGE Annual Conference and Exhibition, Vienna, Austria, 23-26 May, 2011.

Naderi, M., Rostami, B., Khosravi, M. Effect of heterogeneity on the productivity of vertical, deviated and horizontal wells in water drive gas reservoirs. Journal of Natural Gas Science and Engineering, 2015, 23: 481-491.

Newley, T. M. J., Begg, S. H. Characterizing the effects of heterogeneity on oil recovery by dry gas injection. Paper SPE 24921 Presented at the SPE Annual Technical Conference and Exhibition, Washington, D.C., 4-7 October, 1992.

Pandey, S. N., Chaudhuri, A., Rajaram, H., et al. Fracture transmissivity evolution due to silica dissolution/precip-

itation during geothermal heat extraction. Geothermics, 2015, 57: 111-126.

Panja, P., McLennan, J., Green, S. Temperature and pressure profiles for geothermal battery energy storage in sedimentary basins. Paper ARMA 2020 1411 Presented at the 54th U.S. Rock Mechanics/Geomechanics Symposium, physical event cancelled, 28 June-1 July, 2020.

Panja, P., McLennan, J., Green, S. Influence of permeability anisotropy and layering on geothermal battery energy storage. Geothermics, 2021, 90: 101998.

Vargas-Guzmán, J. A. Unbiased estimation of intrinsic permeability with cumulants beyond the lognormal assumption. SPE Journal, 2009, 14(4): 805-810.

Wang, C., Huang, Z., Lu, Y., et al. Influences of reservoir heterogeneity and anisotropy on CO_2 sequestration and heat extraction for CO_2-based enhanced geothermal system. Journal of Thermal Science, 2019, 28(2): 319-325.

Wendt, D., Huang, H., Zhu, G., et al. Geologic thermal energy storage of solar heat to provide a source of dispatchable renewable power and seasonal energy storage capacity. Paper Presented at the Geothermal Resources Council (GRC) Annual Meeting and Expo, Palm Springs, California, 15-18 September 2019.

Wendt, D. S., Huang, H., Zhu, G., et al. Flexible geothermal power generation utilizing geologic thermal energy storage: Final seedling project report. Idaho National Laboratory, United States, 2019b.

Xu, T., Zhu, H., Feng, G., et al. On fluid and thermal dynamics in a heterogeneous CO_2 plume geothermal reservoir. Geofluids, 2017, 2017: 9692517.

Yang, G., Butler, R. M. Effects of reservoir heterogeneities on heavy oil recovery by steam-assisted gravity drainage. Journal of Canadian Petroleum Technology, 1992, 31(8): 37-43.

Appendix A: Heat and fluid flow equations

STARS is CMG's (CMGL, 2021) thermal simulator where simultaneous fluid and heat equations are numerically solved. The simulator has the capability of chemical/polymer flooding, thermal applications, steam injection, horizontal wells, flexible grids, fire flood, etc.

The simplified conservation equation of fluid flow ignoring reaction, mass diffusivity, adsorption, and aquifer equations is given in Eq. (A.1) (space terms are discretized).

$$\frac{\partial}{\partial t}[V_f(\rho_w S_w w_i + \rho_o S_o x_i + \rho_g S_g y_i)] = \sum_{k=1}^{n_f}[T_w \rho_w w_i \Delta\Phi_w + T_o \rho_o x_i \Delta\Phi_o + T_g \rho_g y_i \Delta\Phi_g] + \rho_w q_{wk} w_i + \rho_o q_{ok} x_i + \rho_g q_{gk} y_i \quad \text{(A.1)}$$

(only for well layer k)

The simplified conservation equation of energy flow ignoring reaction, adsorption, heat loss source/sink terms, and thermal aquifer equations is given in Eq. (A.2) (space terms are discretized).

$$\begin{aligned}\frac{\partial}{\partial t}[V_f(\rho_w S_w U_w + \rho_o S_o U_o + \rho_g S_g U_g) + V_r U_r] = &\sum_{k=1}^{n_f}[T_w \rho_w H_w \Delta\Phi_w + T_o \rho_o H_o \Delta\Phi_o + T_g \rho_g H_g \Delta\Phi_g] \\ &+ \sum_{k=1}^{n_f} K\Delta T + \rho_w q_{wk} H_w + \rho_o q_{ok} H_o + \rho_g q_{gk} H_g \qquad \text{(only for well layer k)}\end{aligned} \quad \text{(A.2)}$$

The phase equilibrium relationship can be found in the user manual (CMGL, 2021). Other basic relationships for the flow of fluid and energy in a porous medium are discussed in many reservoir engineering textbooks (Dake, 1983; Ahmed, 2010).

Nomenclature

n_f = number of neighboring regions or grid block faces
q_{jk} = well phase rate on k^{th} layer
S_j = fluid phase saturation
ρ_j = fluid phase molar density
U_j = internal energy
U_r = energy per rock volume
V_f = total volume of fluid phases
V_r = solid rock volume
w_i = mole fraction of i^{th} component in water phase
x_i = mole fraction of i^{th} component in oil phase
y_i = mole fraction of i^{th} component in gas phase
$T_j = Tk_{rj}/(\mu_j r_j)$ phase transmissibilities
T = flow transmissibility between the two regions
k_{rj} = relative permeability of j^{th} phase
μ_j = viscosity
r_j = phase resistance factors, normally 1.0
H_j = phase enthalpy
$\Phi_j = p_j - \rho_j g h$, fluid potential
K = thermal transmissibility between the two regions
ΔT = temperature difference

Subscript

j = w (water), o (oil), g (gas), and s (solid)